Experimental studies of linear quadratic regulator (LQR) cost matrices weighting to control an accurate take-off position of bicopter unmanned aerial vehicles (UAVs)

Jalu Ahmad Prakosa [a, *], Hai Wang [b], Edi Kurniawan [a], Swivano Agmal [c], Muhammad Jauhar Kholili [c]

[a] Research Center for Photonics, National Research and Innovation Agency (BRIN)
PUSPIPTEK, South Tangerang City, Indonesia
[b] Discipline of Engineering and Energy, Murdoch University
90 South Street, Murdoch, Western Australia, 6150, Australia
[c] Research Center for Quantum Physics, National Research and Innovation Agency (BRIN)
PUSPIPTEK, South Tangerang City, Indonesia

Abstract

Controller design for airplane flight control is challenged to achieve an optimum result, particularly for safety purposes. The experiment evaluated the linear quadratic regulator (LQR) method to research the optimal gain of proportional-integral-derivative (PID) to hover accurately the bicopter model by minimizing error. The 3 degree of freedom (DOF) helicopter facility is a suitable bicopter experimental simulator to test its complex multiple input multiple output (MIMO) flight control model to respond to the challenge of multipurpose drone control strategies. The art of LQR setting is how to search for appropriate cost matrices scaling to optimize results. This study aims to accurately optimize take-off position control of the bicopter model by investigating LQR cost matrices variation in actual experiments. From the experimental results of weighted matrix variation on the bicopter simulator, the proposed LQR method has been successfully applied to achieve asymptotic stability of roll angle, although it yielded a significant overshoot. Moreover, the overshoot errors had good linearity to weighting variation. Despite that, the implementation of cost matrices is limited in the real bicopter experiment, and there are appropriate values for achieving an optimal accuracy. Moreover, the unstable step response of the controlled angle occurred because of excessive weighting.

Keywords: experimental evaluation; cost matrices; LQR; bicopter; MIMO flight control.

I. Introduction

Research aircraft flight control [1] is complicated due to its dynamic behavior and uncertainties. The nonlinear behavior of plants also must be taken to account. Not only rotors [2], [3] characteristics but also aerodynamic behaviors of aircraft cause its uncertainty and dynamic. Besides, it must control an airplane's rotation angles in three dimensions: pitch, roll, and yaw. Interaxis coupling between angles adds a more complex task [4]. Because of these reasons, flight control is an exciting research topic.

Flight control has a vital role in running unmanned aerial vehicles (UAVs) [5], [6] well, becoming famous today. The application of UAVs in remote sensing, surveillance, and disaster mitigation has gained more attention because of their relatively low cost, more accurate, and higher maneuvers possibility than on-board pilots [1]. The excellent development of UAVs flight control can ensure its application successfully, although the major use of DC motors provides challenges.

The helicopter is a UAV type with excellent maneuverability and versatility for flight control studies. Moreover, this type has more advantages than fixed wings UAVs in smaller landing areas [7]. Bicopter is a helicopter-type with two rotors on both

* Corresponding Author. Tel: +62-8888311358
E-mail address: jalu.ahmad.prakosa@brin.go.id

Figure 1. The experimental platform of 3 DOF helicopter as bicopter simulator

arms for its maneuver, which is famously implemented by the Chinook helicopter [8]. The plant of 3 DOF helicopters for the laboratory, which Quanser Consulting Inc. develops, is a useful experimental tool to test the flight control method strategies for the bicopter model [9]. Two propellers to generate thrust for lifting the helicopter are driven by both DC motors. The aircraft has free movement to pitch from its center on one side of the arm. Moreover, the arm allows the helicopter body to move in the elevation and yaw directions. Here is Figure 1, which describes the bicopter simulator.

Figure 1 shows that a counterweight is used as a balancing from the propellers. Encoder sensors install some joints; therefore, the helicopter's angular rotation, namely pitch, roll, and yaw, can be measured accurately as feedback elements. The data acquisition is connected between the personal computer (PC) and motor through a driver and amplifier. The pitch, roll, and yaw measurement is delivered via its data acquisition to PC. The application software of MATLAB Simulink can be used to design the flight control technique due to its accessibility to the plant. Hence, the 3 DOF helicopter is a suitable experimental platform to test and validate new flight control strategies to deal with dynamic behavior, nonlinearities, and the helicopter's uncertainties as a UAV plant.

Besides implementing adaptive control with LQR [10] to deal with dynamic behavior, nonlinearities, and uncertainties, the method of optimal control can also be used. Optimal control is a method to achieve the desired dynamic and deal with researching a control law system over a while to optimize an objective function. Some researchers applied many optimal control theories to the helicopter as an object. The application of the H-infinity optimal control [3] approach was analyzed to solve high-order unmodeled dynamics on a helicopter. Sliding Mode Control [11] was simulated and studied for a laboratory helicopter of 3 DOF [12]. Robust LQR attitude control [13], [14] was built for aggressive maneuvers on 3 DOF helicopters, both theory and experiment [15]. LQR theory minimizes the cost function to solve dynamic system operation, commonly implemented in flight control [16].

The research of cost matrices variation of LQR algorithm for flight control [17] is not only exciting but also challenging to be conducted. The weighting of cost matrices [18] supplied by an engineer may have different behavior on another plant. The platform of 3 DOF helicopters should be used to study experimentally optimal flight control strategies for UAV type of bicopter [19]. This research aims to investigate the cost matrices variation of LQR theory to evaluate the most accurate flight control experimentally for the bicopter plant as an optimization strategy. The efficient weighting on cost matrices should be analyzed to achieve optimal flight control strategies [20]. The optimal desire can be obtained by minimizing its error or cost function in the LQR term. Therefore, the accurate position of the helicopter must be achieved to ensure its safety. In addition, it would succeed the application of UAV. Besides, the following points provide a summary of our contributions:

- Demonstrate MIMO control system of the bicopter model through PID controller signal.
- Test the strategies of optimal control theory on experimental tools of 3 DOF helicopters as the bicopter simulator.
- Investigate cost matrices weighting variation of LQR optimization calculation.
- Assess the accuracy of flight position on the LQR method through each error.
- Develop cost matrices of LQR calculation to get minimal errors of angle control from bicopter experimental results.

This activity is conducted as the following: Section II indicates the modeling of the bicopter system. Cost matrices variation of LQR calculation is investigated and discussed in Section III as experimental evaluation. Finally, Section IV presents the conclusion of this work.

II. Materials and Methods

A. Design and method

The angles of rotation of 3-DOF helicopter is analogous with Chinook bicopter description; therefore, the pitch, roll, and yaw can be seen in Figure 2 as general aircraft flight control below:

The set of the angle's rotation for flight control of Chinook's bicopter in Figure 2 is implemented to the 3 DOF helicopter facilities. Its free body diagram is illustrated in Figure 3.
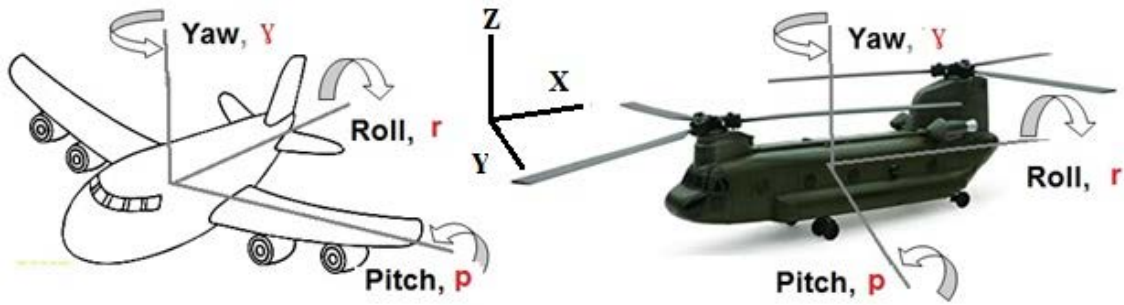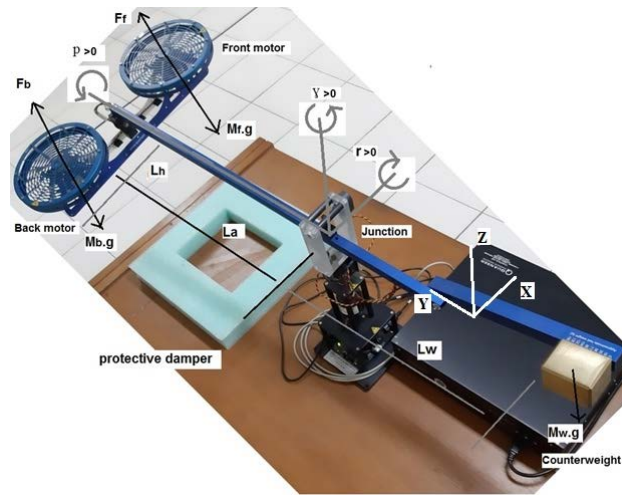
Figure 2. Angles rotation of bicopter

Figure 3. Free body diagram of 3 DOF helicopter

The angles of rotation and the force illustration are described in Figure 3. The signs of each axis for angles of rotation are determined below:

a) The roll angle lies in the direction of the X-axis rotation. The horizontal position of a helicopter if r(t)=0, then roll angle becomes positive, r(t)>0, a helicopter flies higher than counterweight.

b) The yaw angle is in the direction of the Z-axis rotation. The yaw angle is positive, ɣ(t)>0, if it rotates counterclockwise (CCW) direction.

c) The pitch angle is situated in the direction of the Y-axis rotation. The pitch angle increases positively, p(t)>0, when the front motor is higher than the back motor.

The Newton's Law I works when the helicopter hovers stationary or moves at a steady speed. Because of that reason, the whole force sum on the free body diagram of the helicopter is zero when it hovers. Those circumstances are illustrated in equations (1), (2), (3), and (4).

$$\Delta F = F_T - F_W = 0 \qquad (1)$$

The total torque is also zero.

$$\Delta \tau = \tau_T - \tau_W = 0 \qquad (2)$$

$$2V_o L_a K_f = (L_w m_w - L_a m_f - L_a m_b)g \qquad (3)$$

$$V_o = \frac{(L_w m_w - L_a m_f - L_a m_b)g}{2L_a K_f} \qquad (4)$$

The equation (4) shows the voltage (Vo) produced by the amplifier to drive the DC motor. The mathematical model of control systems design for analysis usually uses a state-space model that applies state variables to describe a system by a set of first-order differential or difference equations in equation (5) and Figure 4.

$$\dot{x} = Ax + Bu; y = Cx + Du \qquad (5)$$

where: x = state vector; y = output vector; u = input vector; A = state matrix; B = input matrix; C = output matrix; D = feedforward matrix.

The state vector is defined as equation (6):

$$x^T = \begin{bmatrix} r & p & \gamma & \dot{r} & \dot{p} & \dot{\gamma} \end{bmatrix} \qquad (6)$$

On the other hand, the output vector can be written as (7):

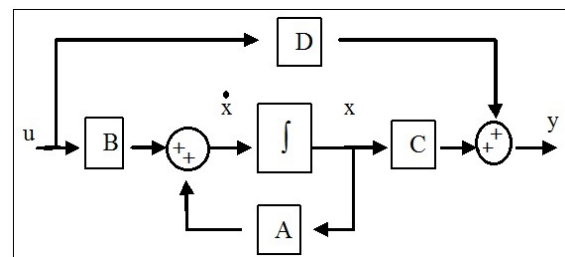$$y^T = \begin{bmatrix} r & p & \gamma \end{bmatrix} \qquad (7)$$

Figure 4. State-space model

Furthermore, the other state-space matrices are set in equation (8), (9), (10), and (11):

A =

$$\begin{bmatrix} 0 & 0 & 0 & 1 & 0 & 0 \\ 0 & 0 & 0 & 0 & 1 & 0 \\ 0 & 0 & 0 & 0 & 0 & 1 \\ 0 & 0 & 0 & 0 & 0 & 0 \\ 0 & 0 & 0 & 0 & 0 & 0 \\ 0 & \dfrac{(L_w.m_w - L_a.m_f - L_a.m_b).g}{m_w.L_w^2 + 2.m_f.L_h^2 + 2.m_f.L_a^2} & 0 & 0 & 0 & 0 \end{bmatrix} \quad (8)$$

B =

$$\begin{bmatrix} 0 & 0 \\ 0 & 0 \\ 0 & 0 \\ \dfrac{L_a.K_f}{m_w.L_w^2 + 2.m_f.L_a^2} & \dfrac{L_a.K_f}{m_w.L_w^2 + 2.m_f.L_a^2} \\ \dfrac{K_f}{2.m_f.L_h^2} & -\dfrac{K_f}{2.m_f.L_h^2} \\ 0 & 0 \end{bmatrix} \quad (9)$$

$$C = \begin{bmatrix} 1 & 0 & 0 & 0 & 0 & 0 \\ 0 & 1 & 0 & 0 & 0 & 0 \\ 0 & 0 & 1 & 0 & 0 & 0 \end{bmatrix} \quad (10)$$

$$D = \begin{bmatrix} 0 & 0 \\ 0 & 0 \\ 0 & 0 \end{bmatrix} \quad (11)$$

B. Proposed cost matrices variation of LQR algorithm

The LQR theory applied a mathematical algorithm that minimizes a cost function by weighting factors supplied by an engineer. The sum of the deviations of critical measurements, such as pitch, roll, and yaw on flight control, is often called the cost function. These settings are usually implemented on machines or processes, particularly on airplanes. Further, the LQR algorithm is an automated method of finding an optimal state-feedback controller of close loop systems [21] as shown in Figure 5.

From the state-feedback law in Figure 5, the input vector is indicated in equation (12):

$$u = -Kx \quad (12)$$

State-feedback gains K becomes the optimal gain matrix to minimize the quadratic cost function.
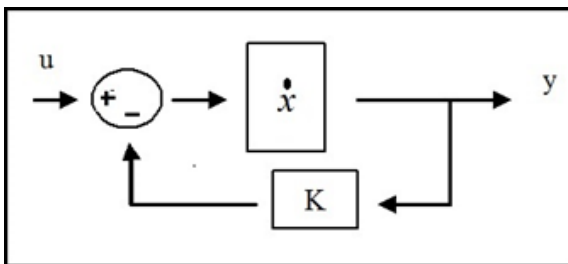

Figure 5. LQR close-loop diagram

Input, u, provides the optimal control signal when the performance index function J is minimized on equation (13). Selecting appropriate weighting matrices Q and R that indicates an important relationship between the state error and control signal in the performance index function aims for the optimal controller design.

$$J(u) = \int_0^\infty (x^T Q x + u^T R u + 2x^T N u)dt \quad (13)$$

Generally, for simple, N is set to 0 (N=0) and becomes equation (14).

$$J(u) = \int_0^\infty (x^T Q x + u^T R u)dt \quad (14)$$

Principally, the optimal gain of LQR can be determined by solving an algebraic Riccati equation. However, it is not efficient in computation time. Therefore, the calculation is held by the application program of MATLAB Simulink. The integrals of the roll and yaw states are included in equation (15) as augmented state vectors from equation (6).

$$x^T = \begin{bmatrix} r & p & \gamma & \dot{r} & \dot{p} & \dot{\gamma} & \int r & \int p \end{bmatrix} \quad (15)$$

Because the updated state vector in equation (15) has eight columns, the cost matrix Q also has an 8x8 matrix size in equation (16).

$$\begin{bmatrix} r & 0 & 0 & 0 & 0 & 0 & 0 & 0 \\ 0 & p & 0 & 0 & 0 & 0 & 0 & 0 \\ 0 & 0 & \gamma & 0 & 0 & 0 & 0 & 0 \\ 0 & 0 & 0 & \dot{r} & 0 & 0 & 0 & 0 \\ 0 & 0 & 0 & 0 & \dot{p} & 0 & 0 & 0 \\ 0 & 0 & 0 & 0 & 0 & \dot{\gamma} & 0 & 0 \\ 0 & 0 & 0 & 0 & 0 & 0 & \int r & 0 \\ 0 & 0 & 0 & 0 & 0 & 0 & 0 & \int p \end{bmatrix} \quad (16)$$

Then the weighting matrix, R, is written in equation (17).

$$R = \begin{bmatrix} c & 0 \\ 0 & c \end{bmatrix} \quad (17)$$

The constant values, c, are chosen 0.01<c<1, for example c=0.05.

State-feedback gains K are calculated by LQR calculation on equation (14) and state-space model of equation (5) to generate PID coefficient gains of motor voltage in equation (18).

K =

$$\begin{bmatrix} K_{1,1} & K_{1,2} & K_{1,3} & K_{1,4} & K_{1,5} & K_{1,6} & K_{1,7} & K_{1,8} \\ K_{2,1} & K_{2,2} & K_{2,3} & K_{2,4} & K_{2,5} & K_{2,6} & K_{2,7} & K_{2,8} \end{bmatrix} \quad (18)$$
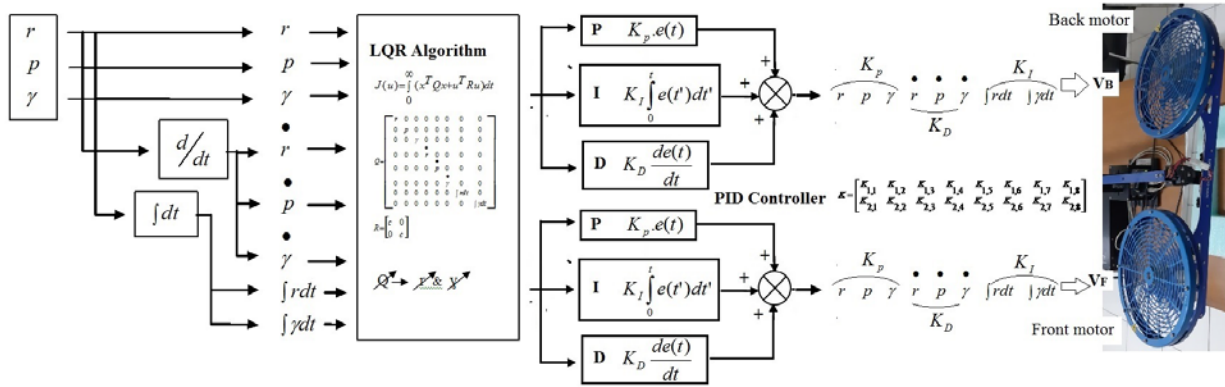
Figure 6. The Overall MIMO control diagram of bicopter

The K matrix on 2x8 indicates the number of rows as output for two motor voltages, namely front motor voltage VF and back motor voltage VB. Further, the number of columns shows the PID gains, which are the third of the first columns for proportional coefficient KP, the following two columns for Derivative coefficient KD, and the last two columns for Integral coefficient KI. Therefore, equation (18) is developed from (15). This MIMO controller [22] of 3 DOF Helicopter can be generally illustrated in Figure 6.

The MIMO [23] diagram (Figure 6) explains clearly why the state-feedback gains K have two rows and eight columns as K2x8. The final outputs are voltages to drive both front and back motor from PID gains of K on equation (18) and motor voltage of Vo on equation (4) as following equation (19):

$$\begin{bmatrix} V_F \\ V_B \end{bmatrix} = K_{2,8} + \begin{bmatrix} V_o \\ V_o \end{bmatrix} \tag{19}$$

Investigation of cost matrices variation on LQR algorithm is proposed to research roll (r) weighting adjustment of Q matrix in the real experiment on bicopter simulator facilities because this angle is directly related to take-off position. The Stochastic Fractal Search (SFS) has been applied to optimize LQR through Q and R weighting matrices in quadcopter simulation [24]. On the other hand, this research wants to investigate weighting matrices variation in an actual experiment of bicopter to optimize its accuracy.

III. Results and Discussions

The variation of cost matrix Q on equation (16) was implemented by weighting adjustment to r angle due to the importance of helicopter take-off circumstances. The factory initially set the roll and yaw by 100 and 10, respectively. Further, the pitch was set to 1 then the other values of derivative and integral followed it. Attentively, the priority of a controlling factor had the heavier weight component due to LQR optimization theory. Hence, r: p: γ= 100: 1:10 meant that the r angle control was more crucial 100 times than p angle control. It also implied that the r angle control was more priority ten times than γ angle control. We only select yaw as the representative angle because of interaxis coupling

between pitch and yaw angles. The prime concern of angle rotation is related to the take-off position of bicopter. The default of matrix Q from equation (16) was filled to equation (20):

$$Q = \begin{bmatrix} 100 & 0 & 0 & 0 & 0 & 0 & 0 & 0 \\ 0 & 1 & 0 & 0 & 0 & 0 & 0 & 0 \\ 0 & 0 & 10 & 0 & 0 & 0 & 0 & 0 \\ 0 & 0 & 0 & 0 & 0 & 0 & 0 & 0 \\ 0 & 0 & 0 & 0 & 0 & 0 & 0 & 0 \\ 0 & 0 & 0 & 0 & 0 & 2 & 0 & 0 \\ 0 & 0 & 0 & 0 & 0 & 0 & 10 & 0 \\ 0 & 0 & 0 & 0 & 0 & 0 & 0 & 0.1 \end{bmatrix} \tag{20}$$

Because of that reason, the variation of r weighting is selected from 25 to 1000 scale. There were three measuring points of r angles at -10°, 0°, and 10°. These angles (Figure 7) were implemented as the take-off position of the helicopter. Time measurement was collected for 20 seconds.

The comparison on more than one angle measuring point must be conducted to ensure the LQR optimal control algorithm's effectiveness on the angle control method. Due to the focus on r angle as the helicopter's take-off position, the other angles, namely p and γ, were set to 0°. Firstly, the experimental results by setting an angle of roll and yaw at -10° are shown in Figure 8 and Figure 9, respectively.

The proposed LQR methods in equations (14), (16), (18), and Figure 6 have successfully controlled both roll and yaw angle at -10° measuring point. The variation of weighting on the Q cost matrix affected the stability of steps response of r angle at -10° setting point. The stability of angle control could be calculated by error, e, which was the difference between a measured angle and a set angle. Besides,
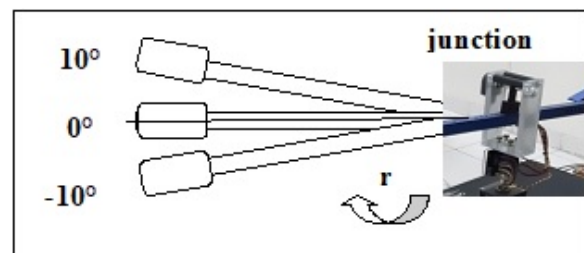

Figure 7. Three measuring points of r angle

the error could be analogous to the cost function, which should be minimized for control optimization in the LQR term. The performance index of the quadratic cost function, J, as in equation (14), was minimized as the error in this research to equation (21).

$$e(t) = \int_{0}^{\infty} (x^T Qx + u^T Ru)dt \qquad (21)$$

All symbols are explained in Table 1. The illustration of cost matrices scaling of LQR theory [18] is described in Figure 10, which aims to minimize error as a equation (21). In other words,

the larger weight of cost matrices [25] was to achieve an optimal accuracy position of angle control. How to find appropriate cost matrices weighting to optimize desired was an art of LQR setting. Figure 8 showed that the proposed LQR method has successfully minimized errors to zero, which achieved asymptotic stability since errors closed to be zero as time ran in unlimited time $\left(\lim_{t \to \infty} \|e\| = 0 \right)$. Moreover, the excessive loading by 1000 produced a huge overshoot helicopter position. It indicated that weighting on cost matrices was only effective for certain values in the real experiment, and if it is exaggerated on weighting, it would decrease the accuracy.
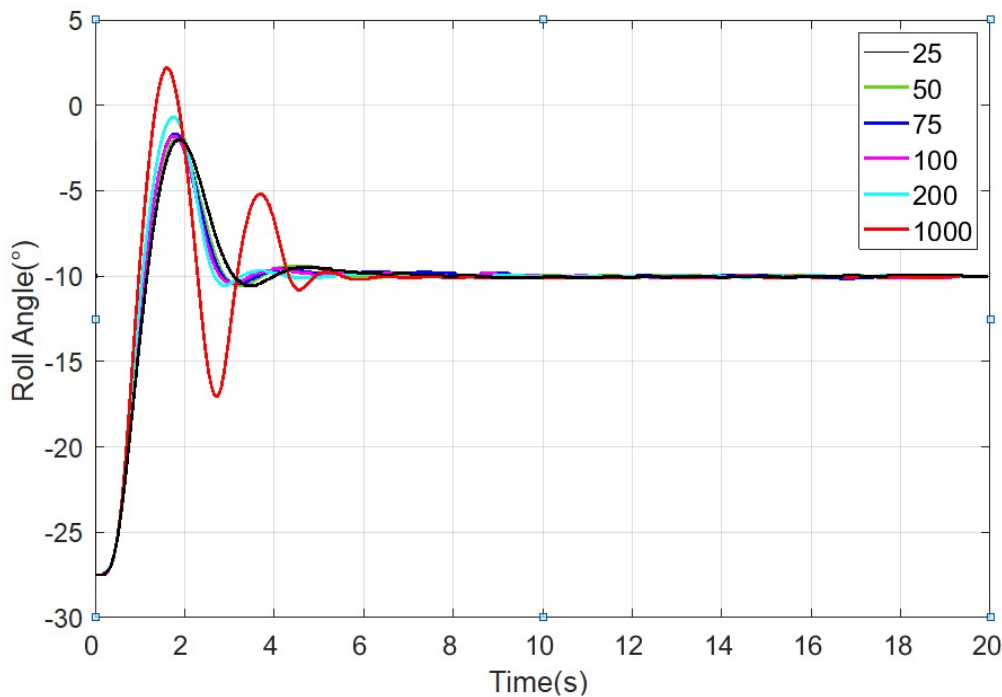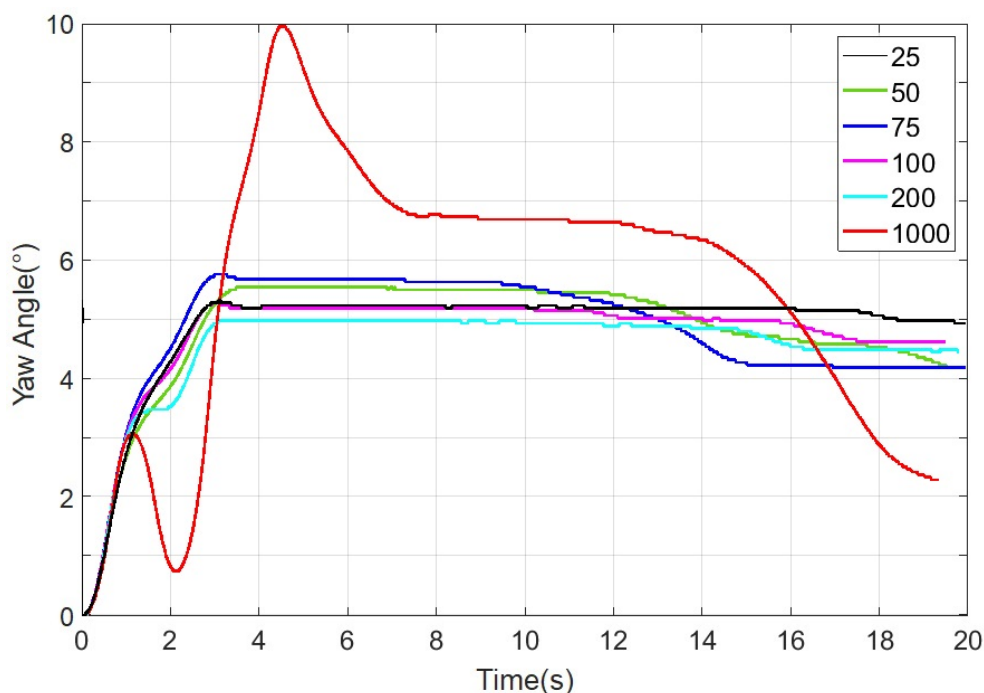

Figure 8. Steps response of roll angle at -10° point

Figure 9. Steps response of yaw angle at -10° point

Table 1.
Symbols description

Parameter	Symbol	Value (Unit)
Roll angle	r(t)	° (degree)
Pitch angle	p(t)	°
Yaw angle	γ(t)	°
Initial error	$e_i(t)$	°
Final error	$e_f(t)$	°
Error	e(t)	°
Gravitation acceleration	g	9.81 m/s²
Thrust force	F_T	N
Thrust torque	τ_W	N.m
Weight	W	N
Torque because of gravitation	τ_T	N.m
Counterweight mass	m_w	1.87 kg
Front motor mass	m_f	0.575 kg
Back motor mass	m_b	0.575 kg
Distance between yaw axis and helicopter body	L_w	0.4699 m
Distance between yaw axis and counterweight	L_a	0.6604 m
Distance between pitch axis and each motor	L_h	0.1778 m
Motor force-thrust constant	K_f	0.1188 N/Volt
Gain constant in two rows and eight columns	K_{2x8}	Volt
Quiescent voltage for motor	V_o	Volt
State vector	x	-
State matrix	A	-
Input matrix	B	-
Output matrix	C	-
Feedforward matrix	D	-
Time	t	Second (s)
State-feedback gain	K	-
Performance index function	J	-
Cost matrix	Q	-
Weighting matrix	R	-
Weighting matrix	N	-
Constant in N matrix	c	-
Front motor voltage	V_F	Volt
Back motor voltage	V_B	Volt
Proportional gain coefficient	K_P	-
Integral gain coefficient	K_I	-
Derivative gain coefficient	K_D	-

Fascinating graphs occurred in Figure 9 which the r weighting variation evidently took effect to γ angle. The peaks of step response on γ angle before 5 s followed the amount of r weighting, which suited the LQR objective. The smaller error at 20 s, e(t), tended to be caused by the larger proportion of
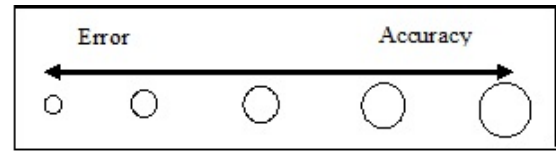

Figure 10. LQR optimization calculation of cost matrices weighting to minimize error or maximize accuracy

Table 2.
Errors analysis of cost matrices variation on LQR algorithm

Weighting variation	Yaw control angle		
	-10°	0°	10°
25	4.92°	2.46°	1.27°
50	4.17°	3.08°	1.76°
75	4.17°	1.93°	3.08°
100	4.61°	1.89°	2.15°
200	4.44°	2.81°	1.63°

r angle variation, except for the 1000 weight condition. Next, the larger control r angle at 0° and 10° has already given the data in Figure 11, Figure 12, Figure 13, and Figure 14.

Although the vast weighting of LQR calculation by 1000 has successfully gotten asymptotic stable at -10°, which errors tend to zero in the time domain, it was not stable for higher angle position by 0° and 10°, respectively. The results characteristic at 10° was not different from the behaviour at 0°. Moreover, the overloading by 1000 scale conducted the unstable bicopter position on both angle points. This case indicated that the weighting factor in the LQR algorithm had limited effectiveness in the actual experiment. For instance, when roll angle was treated by significant cost matrices factor (10) and weighting variation, it should not produce a larger overshoot by heavier weight as the LQR algorithm [26]. The not optimal result would be achieved, but the worst outcome would be treated by excessive weighting. The control inputs in equation (12), for example in 0° point, should be observed further to analyze the cause of overshoot and unstable plant.

Condition of control inputs from amplifier voltage could explain how the overshoots occurred in the bicopter plant in Figure 15. Moreover, an unstable plant might happen because of the saturated signal by 1000 scale. Here is Table 2, which resumed error for only yaw angle because whole roll position points, except in 1000 weight, have achieved zero errors in asymptotic stability for 20 s. The overshoot values and their errors should be investigated not only on cost weighting variation of LQR calculation but also by variation of measured control angle position, as tabulated in Table 3 and Table 4.

Table 3.
Overshoot evaluation of cost matrices variation on LQR algorithm

Weighting variation	Overshoot at measured control angle position					
	r			γ		
	-10°	0°	10°	-10°	0°	10°
25	-2.01°	9.59°	21.98°	5.32°	9.59°	21.98°
50	-2.01°	10.12°	22.69°	5.54°	10.12°	22.69°
75	-1.66°	10.64°	23.13°	5.76°	10.64°	23.13°
100	-1.84°	11.00°	23.56°	5.27°	11.00°	23.56°
200	-0.69°	12.49°	24.88°	4.97°	12.49°	24.88°
1000	2.21°	17.15°	27.06°	9.93°	17.15°	27.06°

Table 4.
Overshoot errors investigation

Weighting variation	Overshoot errors					
	r			γ		
	-10°	0°	10°	-10°	0°	10°
25	7.99°	9.59°	11.98°	15.32°	9.59°	11.98
50	7.99°	10.12°	12.69°	15.54°	10.12°	12.69
75	8.34°	10.64°	13.13°	15.76°	10.64°	13.13
100	8.16°	11.00°	13.56°	15.27°	11.00°	13.56
200	9.31°	12.49°	14.88°	14.97°	12.49°	14.88
1000	12.21°	17.15°	17.06°	19.93°	17.15°	17.06

Overshoot errors mean that difference between overshoot point and the set angle. mean square error (MSE) is the one of performances index to assess the accuracy of experimental results [27]. The purpose of LQR theory is to minimize the cost function, namely error in this case, which can be easier to be investigated by MSE equation (22).
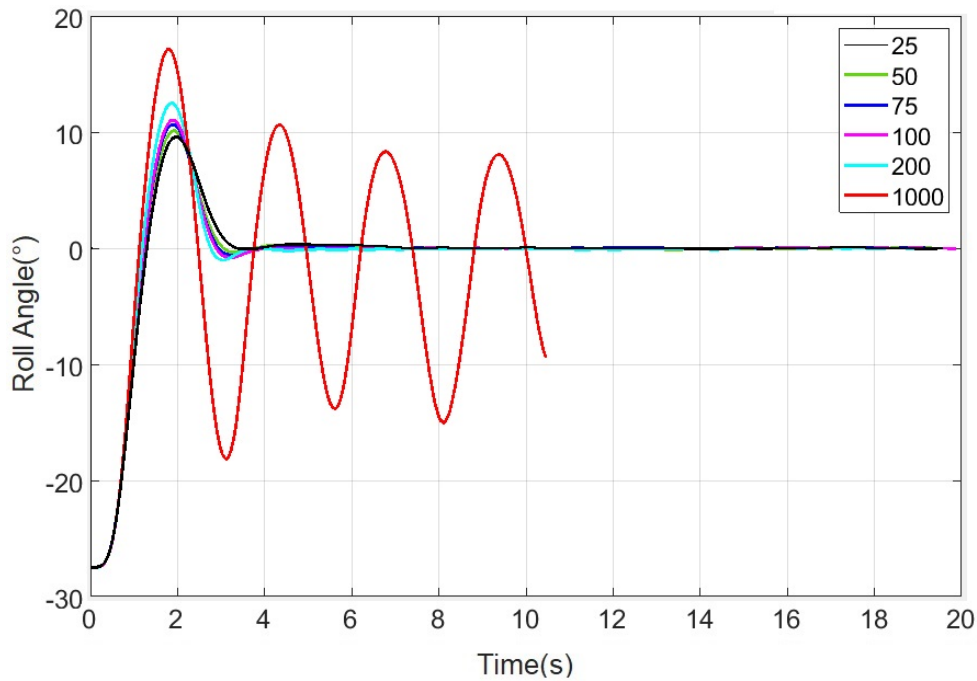

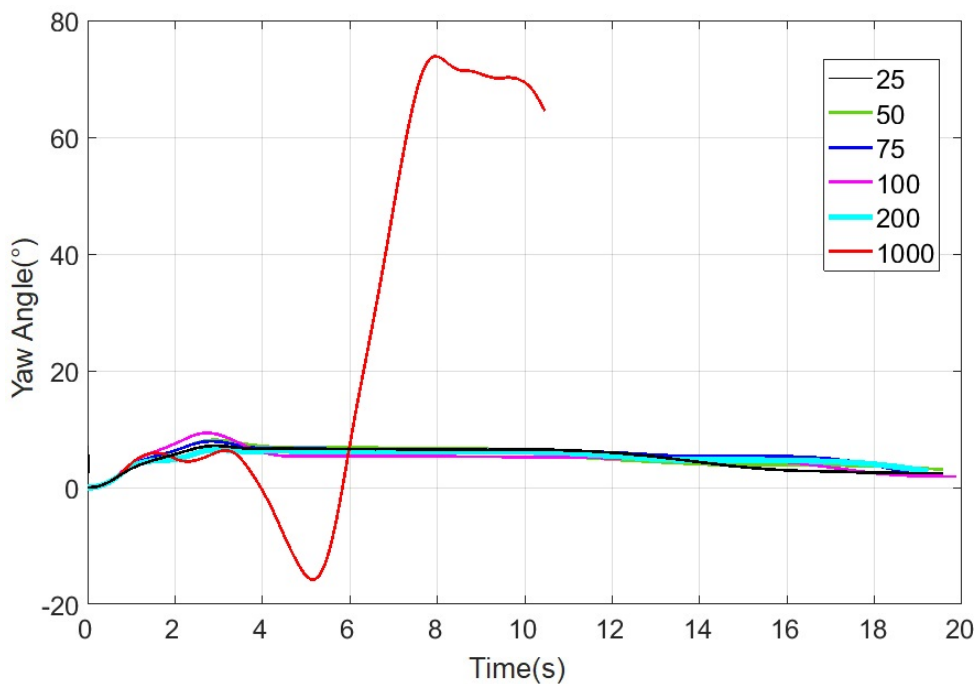Figure 11. Steps response of roll angle at 0° point

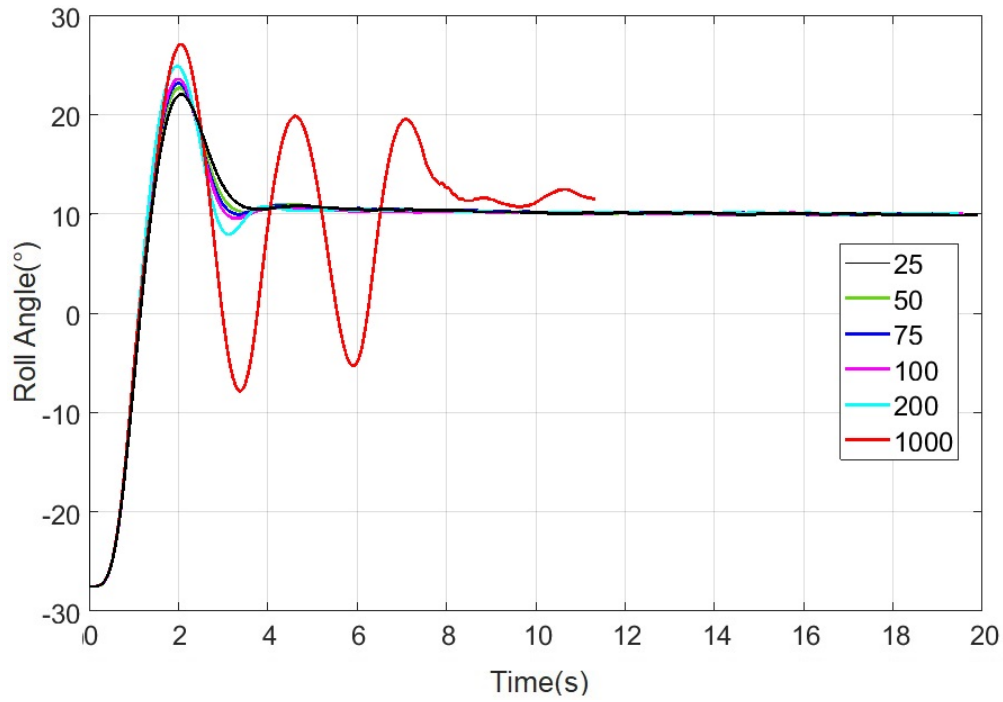Figure 12. Steps response of yaw angle at 0° point

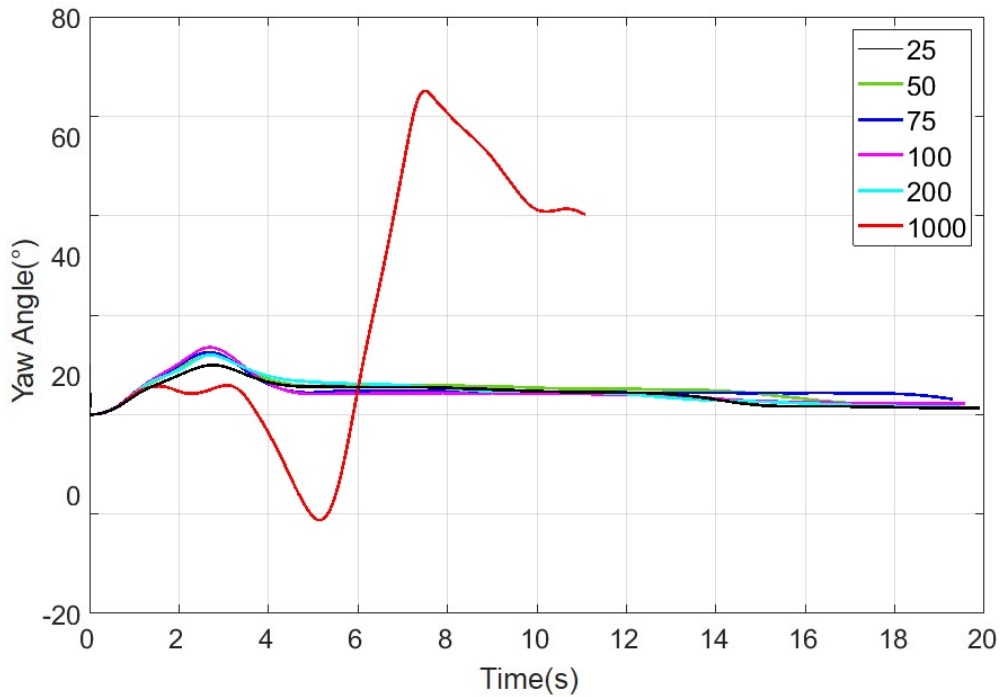Figure 13. Steps response of roll angle at 10° point

Figure 14. Steps response of yaw angle at 10° point

$$MSE = \frac{1}{n} \sum_{i=1}^{n} (e(t))^2 \qquad (22)$$

In this case, the minimum cost function, which was errors, was required to achieve optimal accuracy because the measurement accuracy [21] was essential to assure flight safety. Interestingly, errors in yaw angle measurement in Table 2 indicated that the lower angle position got the higher errors. On the other hand, overshoot errors were larger in a higher angle position in Table 3, which is described for roll and yaw angles in Figure 16 and Figure 17, respectively. Furthermore, the MSE calculations have

different results for various measuring points in Table 5. Nevertheless, the higher weighting tends to yield larger MSE values.

A fascinating event occurred between overshoot errors and weighting, which had excellent linearity by R2 over 0.9. Additionally, the measuring point of 0° achieved the best linearity because it got R2=0.9922 both in roll and yaw angles. The good linearity of both relations might link to the "Linear" term of LQR knowledge, particularly in equation (13). These findings can develop an accurate take-off position of bicopter UAVs according to their needs for future research. The possibility problem was in this case, which achieved the majority of asymptotic

stability because roll angle control position directly corresponded to the primary disturbance of gravitation acceleration, g, as equation (4) (See Figure 3 and Figure 7). Nevertheless, yaw angle errors had an indirect connection to gravitation disturbance so that it produced different results, which took various errors. These observations could inspire building modification method on the LQR technique for accurately hovering bicopter.
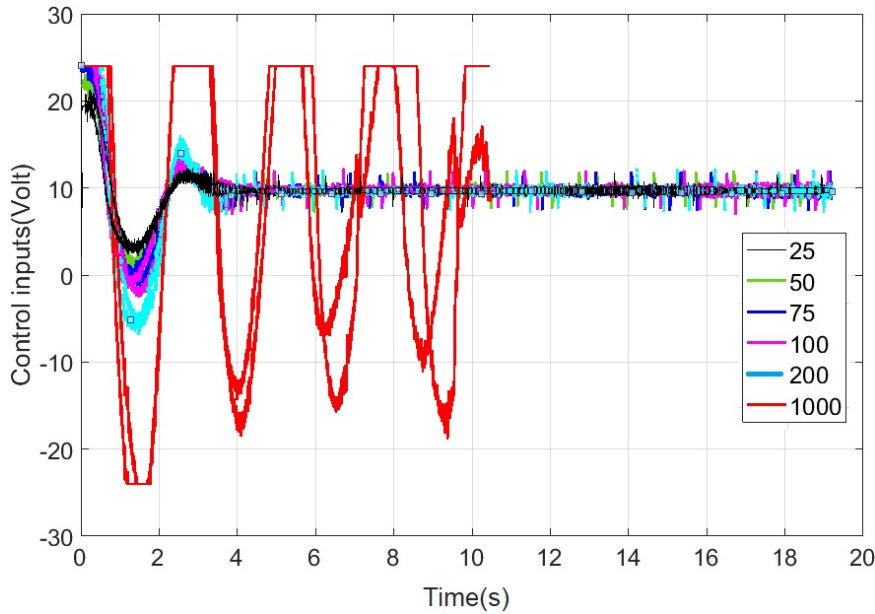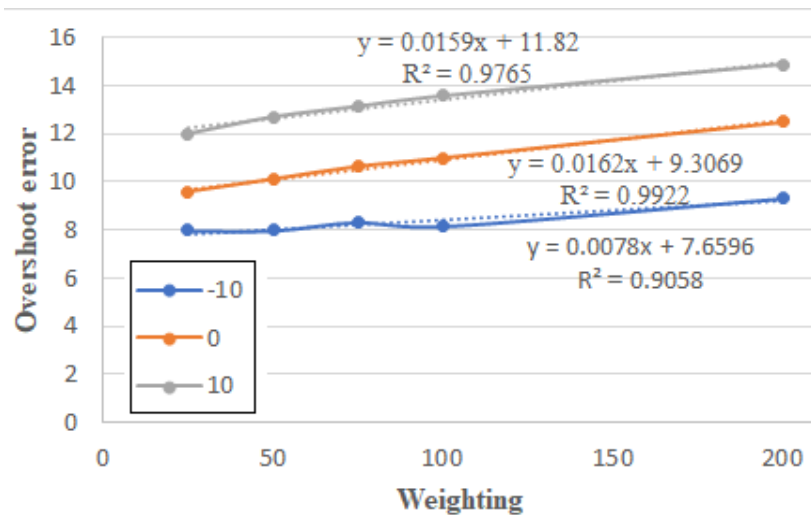

Figure 15. Control inputs

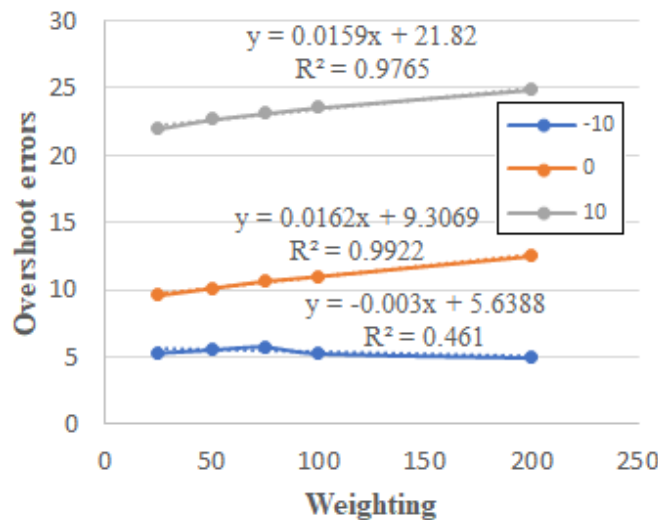Figure 16. Overshoot errors of roll angle relation to weighting variation in different angle position

Figure 17. Overshoot errors of yaw angle relation to weighting variation in different angle position

Table 5.
Mean square error analysis

Weighting variation	Mean square error					
	r			ɣ		
	-10°	0°	10°	-10°	0°	10°
25	12.79°	31.98°	62.01°	24.70°	28.55°	23.04°
50	12.76°	31.86°	64.29°	24.45°	30.27°	32.56°
75	12.56°	32.55°	63.89°	24.20°	34.06°	30.33°
100	12.64°	31.93°	63.42°	23.42°	26.52°	26.63°
200	12.97°	33.85°	64.78°	21.30°	28.26°	28.48°
1000	16.52°	131.08°	155.96°	35.89°	1688.3°	1105°

IV. Conclusion

Experimental data from the bicopter simulator described that the proposed LQR algorithm has successfully controlled angle rotation through PID gains since the heavier weighting factor yielded a more accurate yaw angle. Moreover, the roll control angle achieved asymptotic stability, although it produced large overshoots. Overshoot errors tend to have a linear relation with the weighting variation of LQR cost matrices, particularly for higher angle positions. Despite that, the excessive weighting on controlling roll angle rotation even gave unexpected results, which the larger weight provided the less accurate plant. In addition, the higher weighting tends to produce the larger MSE values. The direct interference from gravitation may cause the difference in the LQR algorithm on flight control optimization between yaw and roll rotation angle. The modified control design and LQR algorithm challenge future research to optimize this UAV position control, especially accuracy optimization.

Acknowledgements

Declarations

Author contribution

J.A. Prakosa: Writing - Original Draft, Writing - Review & Editing, Conceptualization. H. Wang: Conceptualization, Review & Editing. E. Kurniawan: Formal analysis, Conceptualization, Investigation S. Agmal: Visualization, Validation, Data Curation. M.J. Kholili: Resources, Validation.

Funding statement

Competing interest

The authors declare that they have no known competing financial interests or personal relationships that could have appeared to influence the work reported in this paper.

Additional information

Reprints and permission: information is available at https://mev.lipi.go.id/.

Publisher's Note: National Research and Innovation Agency (BRIN) remains neutral with regard to jurisdictional claims in published maps and institutional affiliations.

References

[1] G. Nugroho, Z. Taha, T. S. Nugraha, and H. Hadsanggeni, "Development of a Fixed Wing Unmanned Aerial Vehicle (UAV) for Disaster Area Monitoring and Mapping," *J. Mechatronics, Electr. Power, Veh. Technol.*, vol. 6, no. 2, pp. 83-88, 2015.

[2] J. A. Prakosa, D. V. Samokhvalov, G. R. V. Ponce, and F. S. Al-Mahturi, "Speed control of brushless DC motor for quad copter drone ground test," *2019 IEEE Conference of Russian Young Researchers in Electrical and Electronic Engineering (ElConRus)*, 2019.

[3] J. A. Prakosa, A. Gusrialdi, E. Kurniawan, A. D. Stotckaia, H. Adinanta, and others, "Experimentally robustness improvement of DC motor speed control optimization by H-infinity of mixed-sensitivity synthesis," *Int. J. Dyn. Control*, pp. 1-13, 2022.

[4] I. K. Mohammed and A. I. Abdulla, "Elevation, pitch and travel axis stabilization of 3DOF helicopter with hybrid control system by GA-LQR based PID controller," *Int. J. Electr. Comput. Eng.*, vol. 10, no. 2, p. 1868, 2020.

[5] G. Nugroho and D. Dectaviansyah, "Design, manufacture and performance analysis of an automatic antenna tracker for an unmanned aerial vehicle (UAV)," *J. Mechatronics, Electr. Power, Veh. Technol.*, vol. 9, no. 1, pp. 32-40, 2018.

[6] F. R. Triputra, B. R. Trilaksono, T. Adiono, R. A. Sasongko, and M. Dahsyat, "Nonlinear dynamic modeling of a fixed-wing unmanned aerial vehicle: A case study of Wulung," *J. Mechatronics, Electr. Power, Veh. Technol.*, vol. 6, no. 1, pp. 19-30, 2015.

[7] J. Hu and H. Gu, "Survey on flight control technology for large-scale helicopter," *Int. J. Aerosp. Eng.*, 2017.

[8] J. A. Prakosa, E. Kurniawan, H. Adinanta, S. Suryadi, and M. I. Afandi, "Kajian eksperimen teknik kontrol penerbangan posisi tinggal landas drone bikopter dengan metode PID," *J. Otomasi Kontrol dan Instrumentasi*, vol. 12, no. 2, pp. 1-8, 2020.

[9] J. Apkarian, M. Lévis, and C. Fulford, "Laboratory guide: 3 DOF helicopter experiment for LabVIEW users," Markham: QUANSER, 2012.

[10] O. Saleem, "An enhanced adaptive-LQR procedure for under-actuated systems using relative-rate feedback to dynamically reconfigure the state-weighting-factors," *J. Vib. Control*, p. 10775463221078654, 2022.

[11] U. M. Guzey, E. H. Copur, S. Ozcan, A. C. Arican, B. M. Kocagil, and M. U. Salamci, "Experiment of sliding mode control with nonlinear sliding surface design for a 3-DOF helicopter model," in *2019 XXVII International Conference on Information, Communication and Automation Technologies (ICAT)*, pp. 1-6, 2019.

[12] E. Kurniawan, H. Wang, B. H. Sirenden, J. A. Prakosa, H. Adinanta, and S. Suryadi, "Discrete-time modified repetitive sliding mode control for uncertain linear systems," *Int. J. Adapt. Control Signal Process.*, vol. 35, no. 11, pp. 2245-2258, 2021.

[13] W. Xu, H. Peng, L. Yang, and X. Zhu, "Robust attitude control of a 3-DOF helicopter prototype subject to wind disturbance and communication delay," *Trans. Inst. Meas. Control*, vol. 43, no. 13, pp. 3071-3081, 2021.

[14] T. Dezhi and T. Xiaojun, "Design of UAV attitude controller based on improved robust LQR control," in *2017 32nd Youth Academic Annual Conference of Chinese Association of Automation (YAC)*, pp. 1004-1009, 2017.

[15] X. Yang and X. Zheng, "Adaptive nn backstepping control design for a 3-DOF helicopter: Theory and experiments," *IEEE Trans. Ind. Electron.*, vol. 67, no. 5, pp. 3967-3979, 2019.

[16] X. Zhu and D. Li, "Robust attitude control of a 3-DOF helicopter considering actuator saturation," *Mech. Syst. Signal Process.*, vol. 149, p. 107209, 2021.

[17] M. N. Setiawan, E. R. Suryana, L. Parytta, and W. Andaro, "Pole placement and LQR implementation on longitudinal altitute holding control of wing in surface effect vehicle," *J. Mechatronics, Electr. Power, Veh. Technol.*, vol. 11, no. 2, pp. 86-94, 2020.

[18] E. Joelianto, D. Christian, and A. Samsi, "Swarm control of an unmanned quadrotor model with LQR weighting matrix optimization using genetic algorithm," *J. Mechatronics, Electr. Power, Veh. Technol.*, vol. 11, no. 1, pp. 1-10, 2020.

[19] S. Bai and P. Chirarattananon, "SplitFlyer Air: A Modular Quadcopter That Disassembles into Two Bicopters Mid-Air," *IEEE/ASME Trans. Mechatronics*, 2022.

[20] N. L. Manuel, N. Inanç, and M. Y. Erten, "Control of mobile robot formations using A-star algorithm and artificial potential fields," *J. Mechatronics, Electr. Power, Veh. Technol.*, vol. 12, no. 2, pp. 57-67, 2021.

[21] J. A. Prakosa, A. V. Putov, and A. D. Stotckaia, "Measurement uncertainty of closed loop control system for water flow rate," *2019 XXII International Conference on Soft Computing and Measurements (SCM)*, 2019.

[22] P. Das, R. K. Mehta, and O. P. Roy, "Optimized methods for the pre-eminent performance of LQR control applied in a MIMO system," *Int. J. Dyn. Control*, vol. 7, no. 4, pp. 1501-1520, 2019.

[23] N. Van Chi, "Adaptive feedback linearization control for twin rotor multiple-input multiple-output system," *Int. J. Control. Autom. Syst.*, vol. 15, no. 3, pp. 1267-1274, 2017.

[24] Y. Y. Nazaruddin, I. G. N. A. I. Mandala, and others, "Optimisasi pengontrol LQR menggunakan algoritma stochastic fractal search," in *Seminar Nasional Instrumentasi, Kontrol dan Otomasi*, pp. 235-240, 2018.

[25] A. Iannelli and R. S. Smith, "A multiobjective LQR synthesis approach to dual control for uncertain plants," *IEEE Control Syst. Lett.*, vol. 4, no. 4, pp. 952-957, 2020.

[26] M. Farjadnasab and M. Babazadeh, "Model-free LQR design by Q-function learning," *Automatica*, vol. 137, p. 110060, 2022.

[27] L. Li, Y. Liu, Z. Yang, X. Yang, and K. Li, "Mean-square error constrained approach to robust stochastic iterative learning control," *IET Control Theory & Appl.*, vol. 12, no. 1, pp. 38-44, 2018.